3-D high strength glass-ceramic scaffolds containing fluoroapatite for load-bearing bone portions replacement

3-D high strength glass-ceramic scaffolds containing fluoroapatite for load-bearing bone portions replacement

Francesco Baino*, Enrica Verné , Chiara Vitale-Brovarone

Materials Science and Chemical Engineering Department, Politecnico di Torino, Corso Duca degli Abruzzi 24, 10129 Torino, Italy

*Corresponding author: Francesco Baino

Phone: +39 011 564 4668

Fax: +39 011 564 4699

E-mail: francesco.baino@polito.it

Abstract

This study aimed to fabricate and investigate the structure, mechanical properties and bioactivity of three-dimensional (3-D) glass-ceramic scaffolds for bone tissue engineering. The scaffold material was a fluoroapatite-containing glass-ceramic synthesized by a melting-quenching route. Glass-ceramic powders were mixed with polyethylene particles acting as pores formers; the blend was pressed to obtain "green" compacts that were thermally treated to remove the organic phase and to sinter the inorganic one. The structure and morphology of the resulting scaffolds were characterized by X-ray diffraction, scanning electron microscopy, density measurements and capillarity tests. Crushing tests were carried out to investigate the mechanical properties of the scaffolds. The *in vitro* bioactivity was assessed by soaking the scaffolds in simulated body fluid for different time frames and by analyzing the modifications that occurred on samples surface. The scaffolds had an interconnected macroporous structure with pores up to 50% vol. and they showed an orthotropic mechanical behaviour and strength well above 20 MPa. In addition, *in vitro* tests put into evidence the excellent bioactivity of the material. Therefore, the prepared scaffolds can be used in bone reconstructive surgery as effective load-bearing grafts thanks to their ease of tailoring, bioactive properties and high mechanical strength.

Keywords: Scaffold; Glass-ceramic; High strength; Fluoroapatite; Bioactivity; Bone replacement.

1. Introduction

Bone tissue is usually in need of regeneration or substitution due to tumours removal, trauma or age-related pathologies, such as osteoarthritis and osteoporosis. Two alternatives are possible for bone replacement: (i) transplantation or (ii) implantation.

Transplants can be made by using living or non-living tissues. The commonly recognized "gold standard" in reconstructive bone surgery consists in the use of autografts, that involves harvesting the patient's own tissue from a donor site and transplanting it to the damaged region. Autografts cause no immunological problems but have low availability and can induce death of healthy tissue at the donor site. A partial solution to these drawbacks is the use of allografts, involving the transplant of tissues from another patient or from cadavers. Allografts can cause disease transmission, carry the need of immunosuppressant drugs for the patient and, furthermore, are in short supply.

Implantation involves the replacement of damaged tissues by using, in most cases, man-made biocompatible materials that are designed to act as scaffolds, *i.e.* templates for tissue regeneration and/or remodelling [1].

The general criteria for an ideal bone tissue engineering scaffold can be resumed as follows [2-4]: the scaffold is required to (i) act as a template for bone growth, (ii) produce non-toxic degradation products, (iii) promote osteogenesis by inducing cells adhesion and proliferation, (iv) bond to the host bone creating a stable interface without the formation of scar/fibrous tissue, (v) possess mechanical properties matching those of natural bone, (vi) be tailored to match the shape of the bone defects and (vii) be sterilized according to international standards for commercial production and clinical use.

At present, a scaffold able to fulfil all these requirements does not exist. The major problem concerns the production of scaffolds with porosity comparable to cancellous bone, necessary for graft vascularisation, and satisfactory mechanical strength. Aiming this, bioceramics have been

widely studied and recognized as the most promising materials for scaffolds devoted to bone regeneration.

Hydroxyapatite (HA) has been extensively used for hard-tissue repair due to its chemical and crystallographic similarity to the carbonated apatite in human teeth and bone [5]. Calcium phosphate (CaP) salts, such as β-tricalcium phosphate (β-TCP) or β-calcium pyrophosphate (β-CPP), can act as HA precursors and have usually been adopted as fillers for small bone cavities in orthopaedics and dentistry [6-7]. Both HA and CaP scaffolds exhibit an excellent biocompatibility but are characterized by poor mechanical strength with respect to cancellous bone [8-9].

Bioactive glasses (BGs) and glass-ceramics (BGCs) are, respectively, amorphous or partially crystallized SiO_2-based materials able to bond to living bone stimulating the *in situ* growth of new bone while dissolving over time [10-15]. Bioactivity mechanism was described by Hench in the '70 as the ability to bond to bone and stimulate osteogenesis without drugs or biological agents incorporated into the material [16]. More recently, P_2O_5-based scaffolds, able to resorb at the same time as the bone is repaired, have been proposed [17-20].

BGs and BGCs can be synthesized by conventional melting-quenching routes or sol-gel techniques. Hench demonstrated that, for melt-derived BGs and BGCs, compositions with silica content greater than 60 %wt. are bioinert [21]. However, the ability to bond to bone can be achieved for glasses with up to 90 %mol. silica if the glass is derived by a sol-gel process [22-23].

Scaffolds exhibiting a 3-D interconnected network of macropores above 100 μm, necessary for tissue in-growth and cells migrations into the implant, can be successfully obtained with recent fabrication technologies, such as sol-gel foaming process, starch consolidation, organic phase burning-out and sponge replication [24-29].

At present, BGs and BGCs are used in form of powders or granules as fillers for maxillo-facial surgery and dental applications. Porous scaffolds are suitable as grafts for low-load sites subjected to compression only, such as fused spinal vertebrae. One of the most important challenges is the design and fabrication of high-load bearing scaffolds able to maintain the applied loads for the

required time without showing symptoms of fatigue or failure [2,4]. This challenge has been faced in the present work, in which inorganic scaffolds containing fluoroapatite for bone tissue engineering were produced via a thermally removable phase and characterized from a structural, morphological and mechanical point of view. The bioactivity and biocompatibility of fluoroapatite crystals has been extensively investigated in literature [30-32], and the presence of this phase is expected to impart highly bioactive properties to the proposed glass-ceramic scaffolds.

Glass-ceramic scaffolds combining structural biomimickry with natural bone, remarkable bioactive properties and high-strength features able to actually make them effective load-bearing grafts were successfully produced by very easy technologies of fabrication. Specifically, the method of fabrication was chosen due to its low cost, easiness and versatility for scaffold production. Some considerations for an improvement of scaffold design and tailoring were also presented and discussed at the end of the work.

2. Experimental procedures

2.1. Synthesis and characterization of the starting glass-ceramic

In this work, the basic material used for scaffolding was a silica-based glass-ceramic belonging to the SiO_2-CaO-Na_2O-K_2O-P_2O_5-MgO-CaF_2 system. The glass-ceramic, hereafter referred to as Fa-GC, had the following molar composition: 50% SiO_2, 18% CaO, 7% Na_2O, 7% K_2O, 6% P_2O_5, 3% MgO, 9% CaF_2. The reagents, *i.e.* SiO_2, $Ca_2P_2O_7$, $CaCO_3$, $4MgCO_3Mg(OH)_2{\cdot}5H_2O$, Na_2CO_3, K_2CO_3 and CaF_2, were molten in a platinum crucible in air at 1550 °C for 1 h to ensure homogeneity. The melt was quenched in water to obtain a "frit" that was ground by ball milling and carefully sieved to obtain a powder with grain size below 106 μm.

As-poured Fa-GC was investigated by means of wide-angle (2θ within 10-70°) X-ray diffraction (XRD; X'Pert Philips diffractometer with Bragg-Brentano camera geometry, Cu anode Kα radiation with wavelength λ = 1.5405 Å) to assess the presence of crystalline phases.

2.2. Scaffolds fabrication

Fa-GC-derived scaffolds were prepared by mixing Fa-GC powders sieved below 106 μm with polyethylene (PE) particles that acted as thermally removable pores formers. Fa-GC powders and PE grains were carefully mixed together for 1 h in a polyethylene bottle using a rolls shaker to obtain an effective mixing. Various amounts of PE were added to Fa-GC powders to produce scaffolds with different pores content. Specifically, PE amount was varied from 40 to 70 %vol. to evaluate the best compromise between high porosity content and satisfactory mechanical strength.
Crack-free compacts of powders ("greens") were obtained through uniaxial dry pressing of the mixed powders (130 MPa for 10 s). The "green" bodies were shaped in form of bars (60 × 10 × 10 mm^3) and thermally treated in air (800 °C for 3 h, heating rates set at 5 °C·min^{-1}) to remove the PE powders and to sinter the inorganic phase obtaining macroporous glass-ceramic scaffolds. The sintered bars were cut (Struers Accutom 5 apparatus) to obtain cubic-like macroporous scaffolds.
Fa-GC-derived scaffolds will be named, from now on, with the acronym Fa-GC-S-*P*, where *P* (%vol.) is the volumetric fraction of PE introduced in the starting "green".

2.3. Scaffolds characterization

XRD analysis was carried out on the scaffold reduced in powders to detect the presence of crystalline phases nucleated during the thermal treatment.

Scaffolds morphology and microstructure were evaluated by scanning electron microscopy (SEM, Philips 525 M) to assess the pores size and distribution in the prepared samples; the samples were silver coated before examination.

The scaffolds were carefully polished by SiC grit papers to finally obtain 10 × 10 × 10 mm^3 samples that underwent pores analysis and mechanical testing.

The porosity content Π (%vol.) was assessed by geometrical weight-volume evaluations on five specimens for each series as

$$\Pi = \left(1 - \frac{\rho_s}{\rho_0}\right) \cdot 100,$$

where ρ_s is the apparent density of the scaffold (weight/volume ratio) and ρ_0 is the density of non-porous glass-ceramic.

The interconnection of the pores 3-D network was qualitatively assessed by capillarity tests putting the scaffold into contact with a solution having a viscosity analogous to physiological fluid (30% wt. calf serum and 70%wt. of distilled water [33]). Red ink drops were dispersed to simulate the colour of the blood and to better observe the capillarity up-take of the fluid.

The scaffolds underwent crushing tests (MTS System Corp. apparatus, cross-head speed set at 1.0 $mm \cdot min^{-1}$) carried out on five specimens for each series. The samples were tested in three orthogonal directions, as shown in Figure 1, to put into evidence possible anisotropy of the scaffold. The failure compressive stress σ_f (MPa) was assessed in each direction as

$$\sigma_f = \frac{L}{A},$$

where L (N) is the maximum load registered during the test and A (mm^2) is the cross-sectional area perpendicular to the load axis.

The bioactive properties of the scaffolds was investigated *in vitro* by soaking the samples for different time frames in 30 ml of acellular standard Simulated Body Fluid (SBF) prepared according to Kokubo's protocol [34]. The solution was replaced every 48 h to approximately simulate fluids

circulation in the human body; the pH variations of the solution were daily monitored. The modifications occurring on scaffolds surface was monitored by SEM and compositional (EDS; Edax Philips 9100) investigations.

An easy approach to improve scaffold tailoring was proposed, by using Matlab toolboxes, at the end of the work.

3. Results and discussion

3.1. Starting materials

Compositions belonging to the SiO_2-CaO-Na_2O-K_2O-P_2O_5-MgO-CaF_2 system, in which the nucleation of fluoroapatite is favourite, have been investigated in previous works to obtain bioactive glasses or glass-ceramics [35]. The composition used in the present work was carefully designed in order to promote the nucleation, during quenching, of fluoroapatite crystals.

Figure 2 shows the XRD pattern of as-poured Fa-GC: the main reflections actually corresponding to fluoroapatite were detected, marked and indexed, demonstrating the glass-ceramic nature of the material. The nucleation of fluoroapatite was induced, as foreseen, by the presence of CaF_2 in the starting composition.

SEM investigations on as-poured Fa-GC particle sieved below 106 μm and on PE grains were also carried out. The morphology of Fa-GC particles is non-spherical, irregular and angular as shown in Figure 3a; most of them are within 10-50 μm and only few particles above 50 μm were detected. The PE grains, used as scaffold pores formers, are irregularly shaped and ranged within 50-150 μm (Figure 3b).

3.2. Scaffolds structural and morphological investigations

The thermal treatment, carried out to produce the porous scaffolds, induced the partial crystallization of the residual amorphous phase into a new crystalline phase that was indexed as canasite ($K_3(Na_3Ca_5)Si_{12}O_{30}F_4 \cdot H_2O$), as shown in Figure 4 and previously reported by the authors [33]. The biocompatibility of canasite-containing glass-ceramics has been investigated and demonstrated *in vivo* by other authors [36].

The sintering conditions used for scaffolds fabrication were set at 800°C for 3 h to obtain an effective degree of densification and to impart satisfactory mechanical properties to the scaffold structure.

Fa-GC-scaffolds were produced by using different PE amounts in the range 40-70 %vol. Figure 5 depicts a low-magnification micrograph of Fa-GC-S-40 (face perpendicular to direction T2 in the foreground). Few pores, ranging within 100-200 μm, can be observed. The PE content (*P*) of the starting "greens" was gradually increased till to 70 %vol. to achieve a scaffold porosity comparable to cancellous bone. Scaffolds with $P > 70$ %vol. could not be successfully produced due to scaffold collapse while PE burning-out occurred during the thermal treatment.

The Fa-GC-S-70 cross section shown in Figure 6a reveals an homogeneous pores distribution inside the scaffold; most pores ranged within 100-300 μm, but some pores above 500 μm, probably created by agglomerates of PE particles, are also visible. As clearly depicted in Figure 6b, scaffold trabeculae are characterized by a dispersed microporosity (pores size within 10-20 μm), which is known to play a key role to promote *in vivo* cells adhesion as the osteoblats preferably attach and spread on a rough surface [37].

Pores size plays a crucial role for graft colonization by cells. In fact, it has been demonstrated that well-engineered scaffolds should exhibit pores content and size according to the type and need of the specific cells that could migrate into the implant. Pores above 100 μm allow (i) the scaffold colonization by osteoblasts, whose size is within 10-50 μm, and (ii) an effective scaffold vascularization (nutrients supplying for cells, waste products removal).

3.3. Pores investigations

The total porosity values of the prepared scaffolds, including the contribution of both macropores (> 100 μm) and micropores (< 100 μm), are collected in Table 1. It should be noticed that the actual porosity (Π) is lower than the theoretical one (*P*) due to the scaffold shrinkage that occurred during the thermal treatment. A low standard deviation can be observed for the data reported in Table 1, thus assessing the homogeneous distribution of porosity in the "green" bars and demonstrating the reproducibility of the samples.

Figure 7 reports the result of capillarity tests on Fa-GC-S-70: the fluid went up through scaffold pores network in ~10 s, thus confirming the high interconnection degree of the porous texture. This is a crucial feature to attain a fast viability of the inner parts of the scaffold and to promote an effective *in vivo* bone in-growth [37-38].

3.4. Scaffolds mechanical characterization

An example of Fa-GC-S-70 stress-strain curve (compression along direction T1) is depicted in Figure 8; a similar plot was found for the scaffold with lower pores content. As highlighted in this picture, the curve can be divided in three regions, referred to as I, II and III). Region I exhibits a positive slope (Hookean-like behaviour) that ends with a first peak followed by an apparent stress drop due to the onset of thinner trabeculae cracking. The scaffold was still able to bear higher loads, thus the stress rises again till a second stress peak is reached (region II); the following stress drop corresponds to the fracture of thick trabeculae. In the region III the stress values slowly increase because the densification of the fractured scaffold, progressively reduced in powders, occurs. A similar behaviour was described for glass-ceramic scaffolds obtained via burning-out method but fabricated with a material different from Fa-GC [39]. The failure compressive stresses assessed along the directions A, T1 and T2 (Figure 1) are collected in Table 2. These results are consistent

with the pores content data shown in Table 1: as expected, by increasing the starting PE content the porosity increases too but, at the same time, the scaffold strength gradually decreases. The strengths along the directions T1 and T2 are comparable, whereas the strengths along the direction A are from 3 to 5 times higher than those acquired in the two other directions. Therefore, it is possible to conclude that the scaffolds show a typical orthotropic behaviour. In authors' opinion, scaffolds orthotropy is due to the phenomenon shown in Figure 9. Ought to the pressing of Fa-GC powders/PE particles blend to obtain the "green" compacts, the PE grains are deformed along the bar axis. Therefore, the resulting scaffold pores, that replicated the PE grain size and shape, were preferentially oriented along the bar axis. This involved an increase of resistant area along the direction A in comparison with the directions T1 and T2, thus determining the orthotropic behaviour of the scaffold.

The produced scaffolds exhibit very interesting properties: in fact, they are mechanically orthotropic, which is a feature peculiar to cortical bone, but exhibit a pores content that is one order of magnitude higher than that of compact bone and, in addition, their structure mimics the texture of cancellous bone. The values of mechanical strength, collected in Table 2, are intermediate between those of cancellous (2-12 MPa) and cortical (50-200 MPa) bone [21,40-41]. The high strength is due to the peculiar morphology of Fa-GC-derived scaffolds in which the pores are separated by dense regions; this involves low interconnection degree of the pores. It should be noticed that, at present, the bioceramic scaffolds commonly proposed in literature for bone replacement, such as HA-based and Bioglass®-derived scaffolds [8, 42-43], exhibit lower mechanical strength (below 1 MPa) than that of cancellous bone, and for this reason they are far from an actual clinical use. The features of the proposed Fa-GC-derived scaffolds make them very versatile grafts for bone replacement and they can be successfully proposed for the substitution of extensive bone portions also in load-bearing bone segments.

3.5. Scaffolds in vitro bioactivity

The biocompatibility and bioactivity of fluoroapatite, due to its chemical and crystallographic similarity to bone mineral, have been widely demonstrated in literature. Therefore, the presence of this phase, which is contained in the starting Fa-GC, make by itself the Fa-GC-derived scaffolds biocompatible and bioactive.

In addition, the produced scaffolds are highly bioactive according to the mechanism described by Hench [16]: ion-exchange phenomena between the material and the biological fluids can lead to the precipitation of an apatite layer on the scaffold surface.

After soaking in SBF for 7 days, scaffolds walls are completely covered by globe-shaped agglomerates of a newly formed phase, as shown in Figure 10a. The compositional analysis, reported in Figure 10b, reveals that this phase is constituted by calcium and phosphorus, with Ca/P molar ratio of 1.65, which closely approaches the ratio of natural hydroxyapatite (1.67) in the natural bone. The presence of a hydroxyapatite layer is expected to impart properties of biomimickry to the scaffolds and to promote cells adhesion, as demonstrated by other authors [37]. The variations of pH solution values were moderate: pH increased up to 7.55 after soaking for the first 48 h (reference value for SBF pH: 7.40). For this reason, no cytotoxic effect after *in vivo* implantation is foreseen to be induced by the material.

In this work the scaffolds have been characterized mainly from a structural and mechanical viewpoint; tests devoted to evaluate the biological compatibility of Fa-GC by using osteoblast-like cells (MG63) were reported in a previous work [44] showing a high biocompatibility. Work is in progress to study the effect of ion release on bone cells and it will be the topic of future publications.

3.6. Considerations about scaffold tailoring

As concluding remarks, the authors wish to present and discuss a preliminary approach for improving scaffold design and tailoring.

By adopting a remarkable simplification of the problem, it is possible to tailor the scaffolds, from a structural viewpoint, by knowing the theoretical porosity *P*, *i.e.* the volumetric fraction of PE introduced in the starting "greens", as the only design parameter.

As already mentioned, the actual porosity (Π) was different from the theoretical one (*P*) due to the shrinkage occurring during the thermal treatment. The final pores content can be related to *P* by means of an empirical function interpolating the measured values, that was determined through the LMS algorithm. The easier function fitting the experimental data is a polynomial continuous function of order 2:

$$\Pi^*(P) = -0.012P^2 + 2.22P - 45.86,$$

where Π^* (%vol.) is the expected (calculated) final porosity of the scaffold.

The comparison between the empirical curve and the experimental porosity values is shown in Figure 11.

Likewise, the strength of the scaffolds can also be related to *P* by means of a continuous fitting function. Considering, for instance, the stress along the direction T1, the fitting function is a polynomial function of order 3:

$$\sigma^*(P) = 0.00050P^3 - 0.65P^2 + 1.35P + 74.26,$$

where σ^* (MPa) is the foreseen (calculated) stress of the scaffold (direction T1). The fitting curve for scaffold strength is compared with experimental values in Figure 12.

The empirical curves $\Pi^*(P)$ and $\sigma^*(P)$ can be used for scaffold design in two different ways: (i) by setting *P*, it is possible to foresee the final pores content and strength of FaGC-derived scaffolds, or (ii) by choosing a specific value of porosity/strength (Π^*/σ^*) as a target, it is possible to know the value of *P* which is necessary to achieve that target.

It should be underlined that this approach allows to obtain only rough and preliminary results, because of two main problems: (i) non-ideal samples reproducibility due to experimental conditions

and (ii) intrinsic limits of the fitting curves, that can also lead to results lacking in an actual physical meaning. Concerning the point (ii) an easy example can be presented: if $P \sim 0$ %vol., the scaffold final porosity should also be ~0 %vol., but the corresponding fitting curve gives a non-meaningful negative value ($\Pi^* = -45.86 < 0$).

4. Conclusions

Porous inorganic scaffolds for bone tissue replacement were produced by using bioactive glass-ceramic powders as basic material and polyethylene particles as thermally removable pores formers. The composition of the glass-ceramic was designed to induce the nucleation of highly biocompatible and bioactive fluoroapatite crystals in the final scaffolds. The pores content was tailored by introducing different amounts of polymeric particles in the starting "green" compacts, that underwent a thermal treatment to obtain sintered porous samples having a porosity up to 50% vol.. The fabrication method chosen for scaffolds production led to highly reproducible samples in terms of pores content and mechanical strength.

The 3-D network of interconnected macropores (> 100 μm) is able to promote *in vivo* blood vessels access and cells migration into the scaffolds. In addition, a diffused microporosity, which is known to promote cells adhesion, was observed in all prepared scaffolds. The scaffolds showed a mechanically orthotropic behaviour and a compressive strength well above 20 MPa and thus comparable to natural bone. In addition, the scaffolds exhibited an *in vitro* highly bioactive behaviour, as a thick hydroxyapatite layer was formed on samples surface after soaking in simulated body fluids.

Therefore, the produced scaffolds can be proposed as effective candidates for load-bearing applications in orthopaedics and in the field of bone tissue replacement due to their high mechanical strength, bioactivity and easy tailoring and processability.

Acknowledgements

The authors would like to acknowledge the Ministry of University and Research (MIUR) of Italian Government (PRIN 2006) and Regione Piemonte (Ricerca Sanitaria Finalizzata 2008) for financially supporting this work.

References

[1] L.L. Hench, J.M. Polak, Science 295 (2002) 1014.

[2] D.W. Hutmacher, Biomaterials 21 (2000) 2529.

[3] J.R. Jones, L.L. Hench, J. Biomed. Mater. Res. B 68 (2004) 36.

[4] J.R. Jones, L.M. Ehrenfried, L.L. Hench, Biomaterials 27 (2006) 964.

[5] N. Ozawa, S. Negami, T. Odaka, T. Morii, T. Koshino, J. Mater. Sci. Lett. 8 (1989) 869.

[6] R.Z. LeGeros, Clin. Mater. 14 (1993) 65.

[7] W. Cao, L.L. Hench, Ceram. Int. 22 (1996) 493.

[8] R.C. Thomson, M.J. Yaszemski, JM. Powers, A.G. Mikos, Biomaterials 19 (1998) 1935.

[9] E. Ebaretonbofa, J.R.G. Evans, J. Porous Mater. 9 (2002) 257.

[10] Vogel W, Hoeland W, Naumann K, Gymmel, J. Non-Cyst. Solids 80 (1984) 34.

[11] M.R. Filqueiras, G. LaTorre, L.L. Hench, J. Biomed. Mater. Res. 27 (1993) 445.

[12] L.L. Hench, J. Biomed. Mater. Res. 41 (1998) 511.

[13] L.L. Hench, J. Am. Ceram. Soc. 81 (1998) 1705.

[14] L.L. Hench, Biomaterials 19 (1998) 1419.

[15] L.L. Hench, J. Mater. Sci.: Mater. Med. 17 (2006) 967.

[16] L.L. Hench, R.J. Splinter, W.C. Allen, T.K. Greenlee, J. Biomed. Mater. Res. 5 (1972) 117.

[17] A. Kesisoglou, J.C. Knowles, I. Olsen, J. Mater. Sci.: Mater. Med. 13 (2002) 1189.

[18] J.C. Knowles, J. Mater. Chem. 13 (2003) 2395.

[19] A. Patel, J.C. Knowles, J. Mater. Sci.: Mater. Med. 17 (2006) 937.

[20] E.A. Abou Neel, J.C. Knowles, J. Mater. Sci.: Mater. Med. 19 (2008) 377.

[21] L.L. Hench, J. Wilson, Introduction to bioceramics, World Scientific, Singapore, 1993.

[22] P. Sepulveda, J.R. Jones, L.L. Hench, J. Biomed. Mater. Res. 61 (2002) 301.

[23] M.M. Pereira, J.R. Jones, L.L. Hench, Adv. Appl. Ceram. 104 (2005) 35.

[24] O. Lyckfeldt, J.M.F. Ferreira, J. Eur. Ceram. Soc. 18 (1998) 131.

[25] P. Sepulveda, J.R. Jones, L.L. Hench, J. Biomed. Mater. Res. 59 (2002) 340.

[26] C. Vitale-Brovarone, S. Di Nunzio, O. Bretcanu, E. Verné, J. Mater. Sci.: Mater. Med. 15 (2004) 209.

[27] C. Vitale-Brovarone, E. Verné, L. Robiglio, P. Appendino, F. Bassi, G. Martinasso, G. Muzio, R.A. Canuto, Acta Biomater. 3 (2007) 199.

[28] J.R. Jones, G. Poologasundarampillai, R.C. Atwood, D. Bernard, P.D. Lee, Biomaterials 28 (2007) 1404.

[29] C. Vitale-Brovarone, F. Baino, E. Verné, J Mater. Sci.: Mater. Med. 20 (2009) 643.

[30] C. Vitale-Brovarone, E. Verné, M. Bosetti, C. Moisescu, F. Lupo, S. Spriano, M. Cannas, Biomaterials 23 (2003) 3395.

[31] L.J. Pullen, K.A. Gross, J. Mater. Sci.: Mater. Med. 16 (2005) 399.

[32] X. Chen, L.L. Hench, D. Greenspan, J. Zhong, X. Zhang, Ceram. Int. 24 (2008) 401.

[33] C. Vitale-Brovarone, M. Miola, C. Balagna, E. Verné, Chem. Eng. J. 137 (2007) 129.

[34] T. Kokubo T, H. Takadama, Biomaterials 27 (2006) 2907.

[35] C. Moisescu, C. Jana, S. Habelitz, G. Carl, C. Ruessel, J. Non-Cryst. Solids 248 (1999) 176.

[36] V.M. Da Rocha Barros, L.A. Salata, C.E. Sverzut, S.P. Xavier, R. Van Noort, A Johnson, P.V. Hatton, Biomaterials 23 (2002) 2895.

[37] Z. Schwartz, T.W. Hummert, D.L. Cochran, J. Simpson, D.D. Dean, B.D. Boyan, J. Biomed. Mater. Res. 32 (1996) 55.

[38] D. Rokusek, C. Davitt, A. Bandyopadhyay, S. Bose, H.L. Hosick, J. Biomed. Res. A 75 (2005) 588.

[39] C. Vitale-Brovarone, F. Baino, E. Verné. J. Biomaterials Appl. (2009), doi: 10.1177/0885328208104857.

[40] W. Bonfield, in: G.W. Hastings, P. Ducheyne (Ed.), Natural and Living Biomaterials, CRC Press, Boca Raton (Florida), 1984, p. 43.

[41] S.C. Cowin, in: S.C. Cowin (Ed.), Bone Mechanics, CRC Press, Boca Raton (Florida), 1984, p. 130.

[42] Q.Z. Chen, I.D. Thompson, A.R. Boccaccini, Biomaterials 27 (2006) 2414.

[43] M. Xigeng, D.M. Tan, L. Jian, X. Yin, R. Crawford, Acta Biomater. 4 (2008) 638.

[44] E. Verné, S. Ferraris, M. Miola, G. Fucale, G. Maina, G. Martinasso, R.A. Canuto, S. Di Nunzio, C. Vitale-Brovarone, Adv. Appl. Ceram. 107 (2008) 234

Figure

Fig. 1 Directions of mechanical testing (compression) on final cubic scaffolds: A = direction along the bar axis, T1 and T2 = transversal directions perpendicular to the bar axis

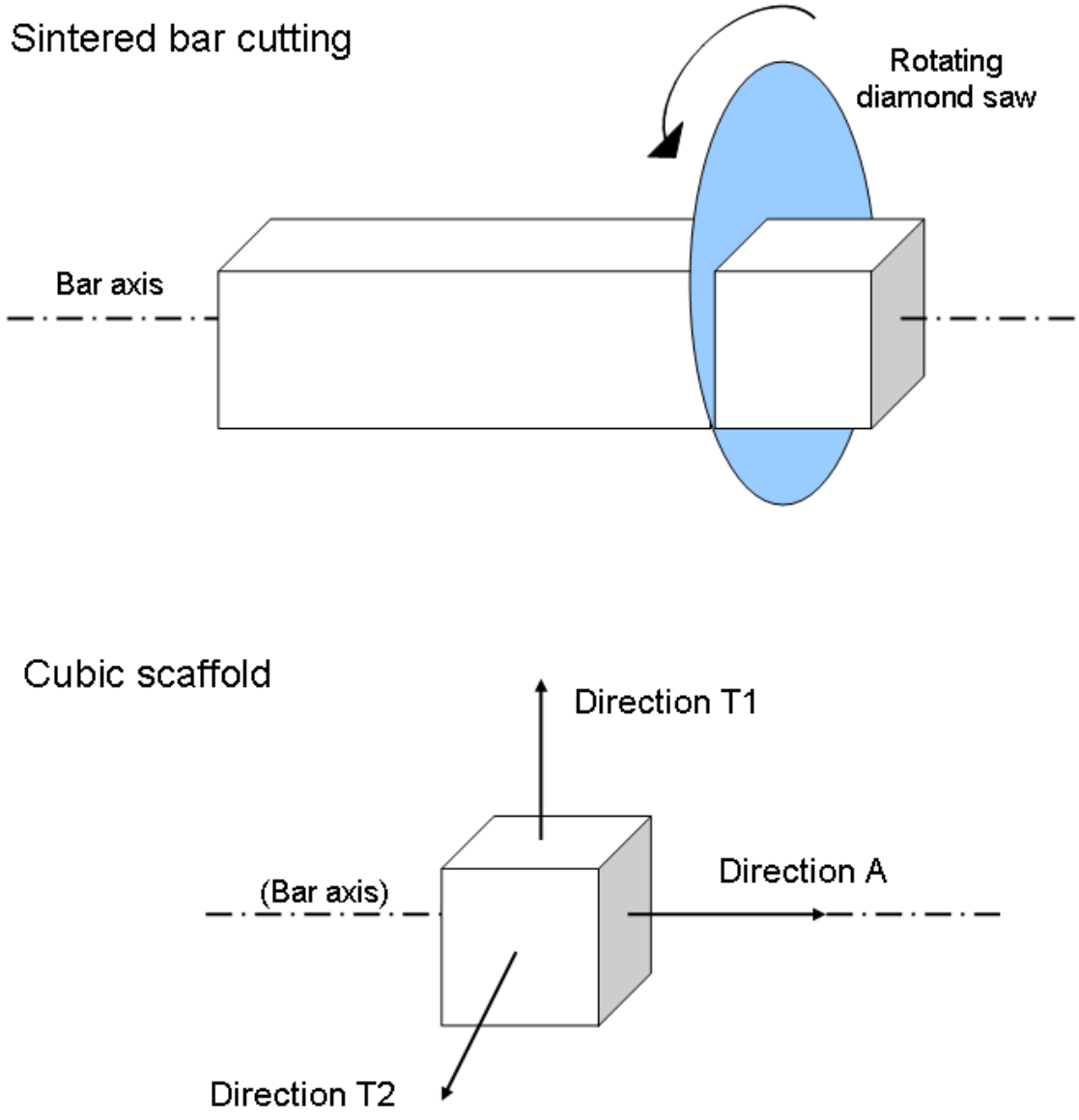

Fig. 2 XRD pattern of as-poured FaGC

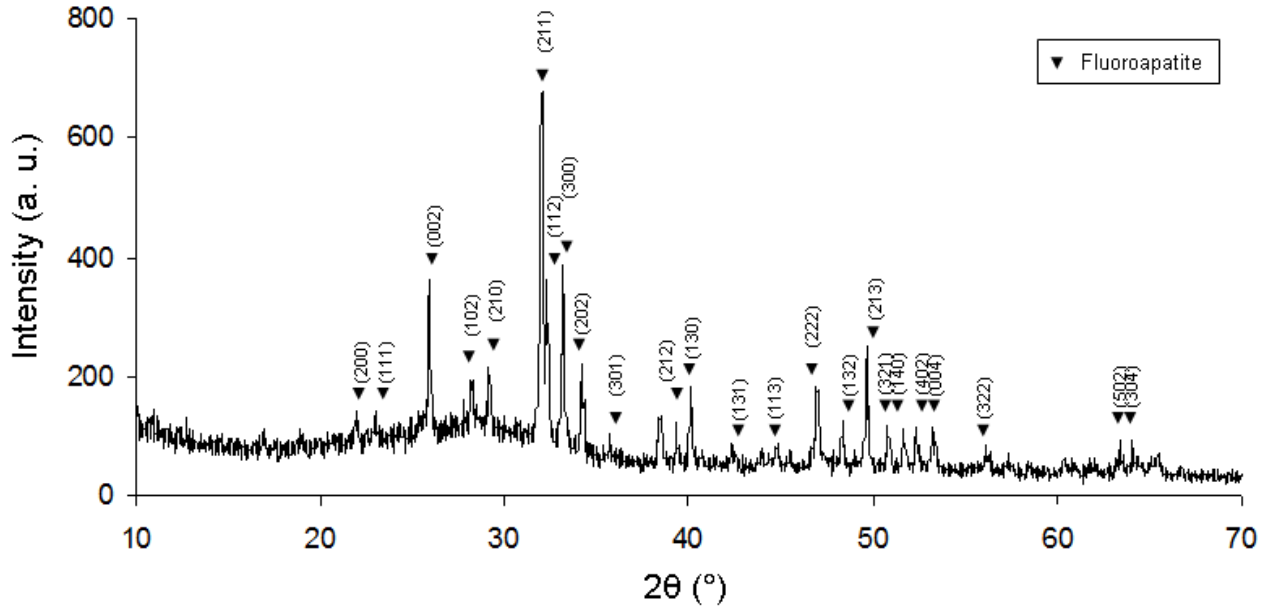

Fig. 3 Starting materials for scaffolding: (a) FaGC powders and (b) PE particles

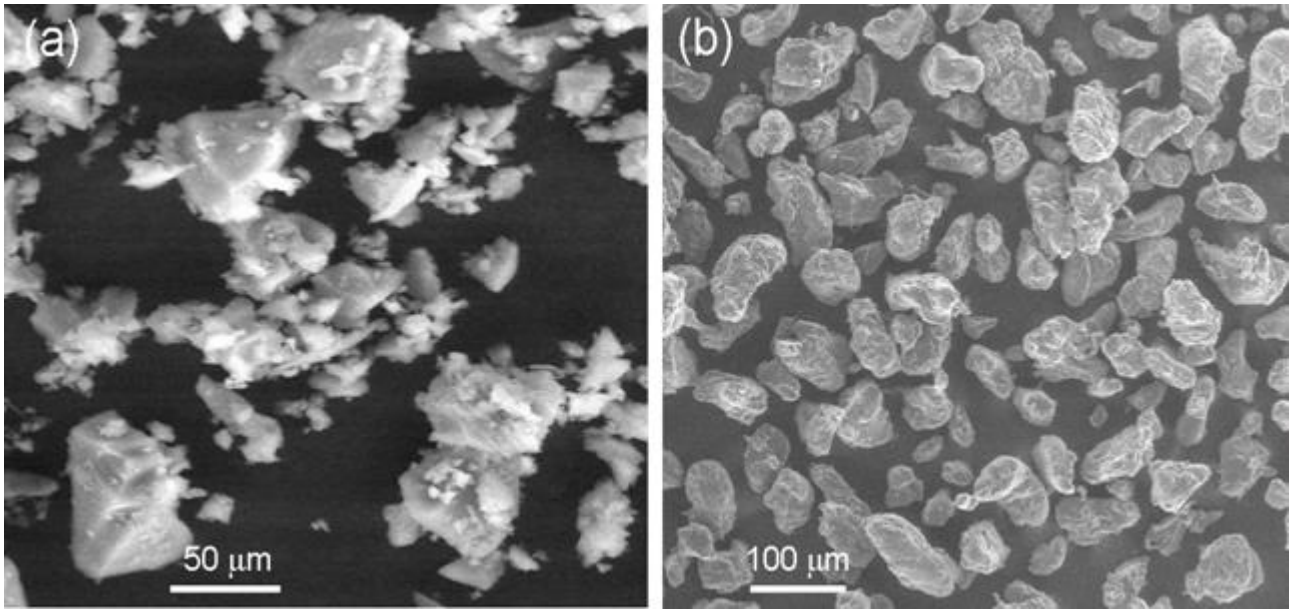

Fig. 4 XRD pattern of ground scaffold

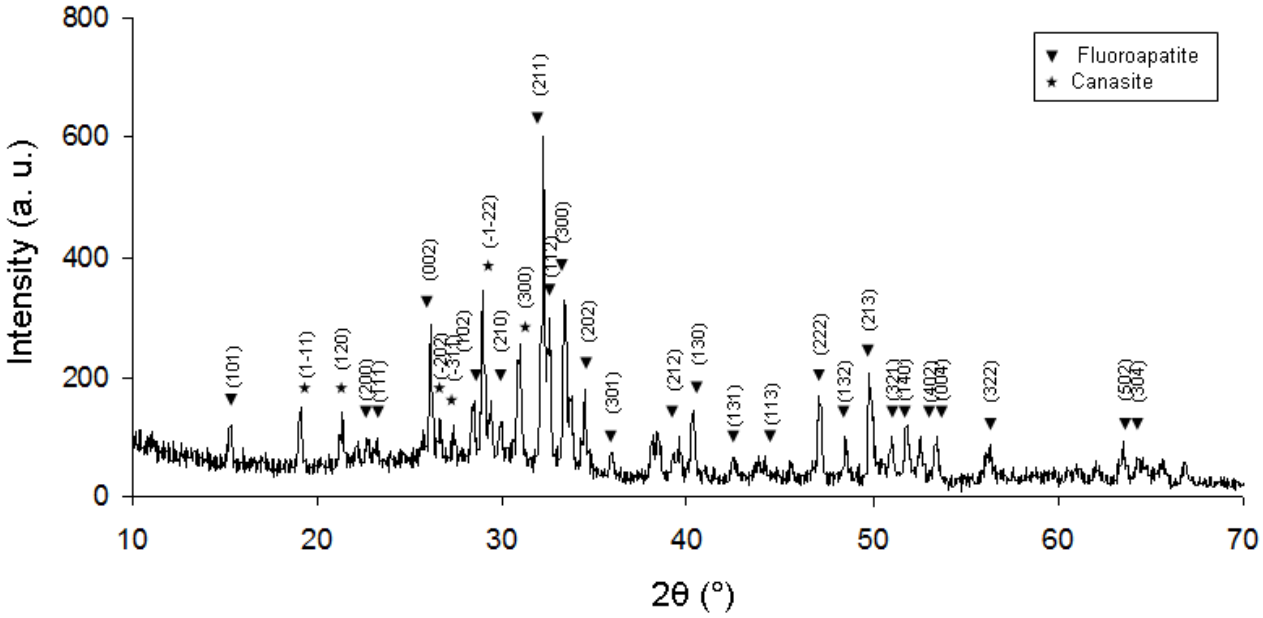

Fig. 5 Low-magnification SEM image of FaGC-S-40

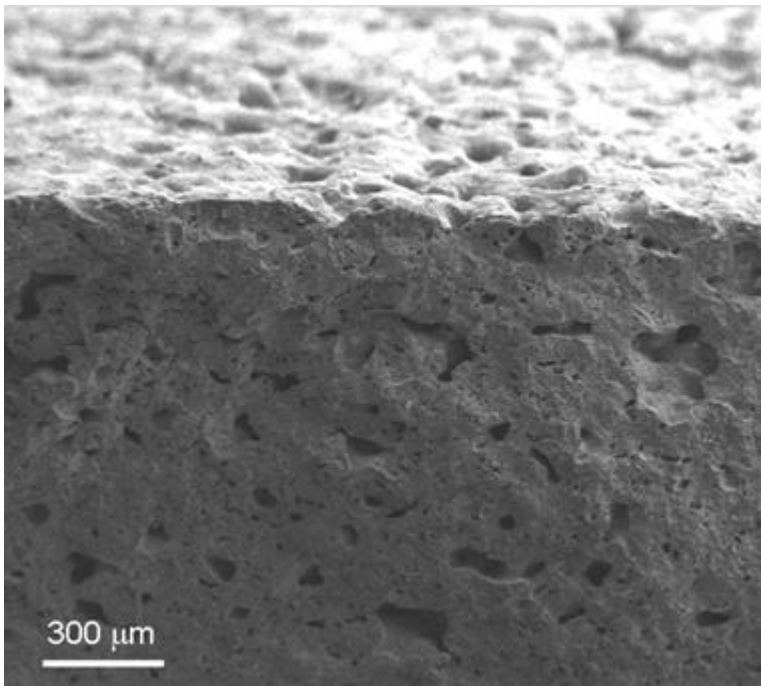

Fig. 6 FaGC-S-70: (a) cross-section and (b) pores magnification

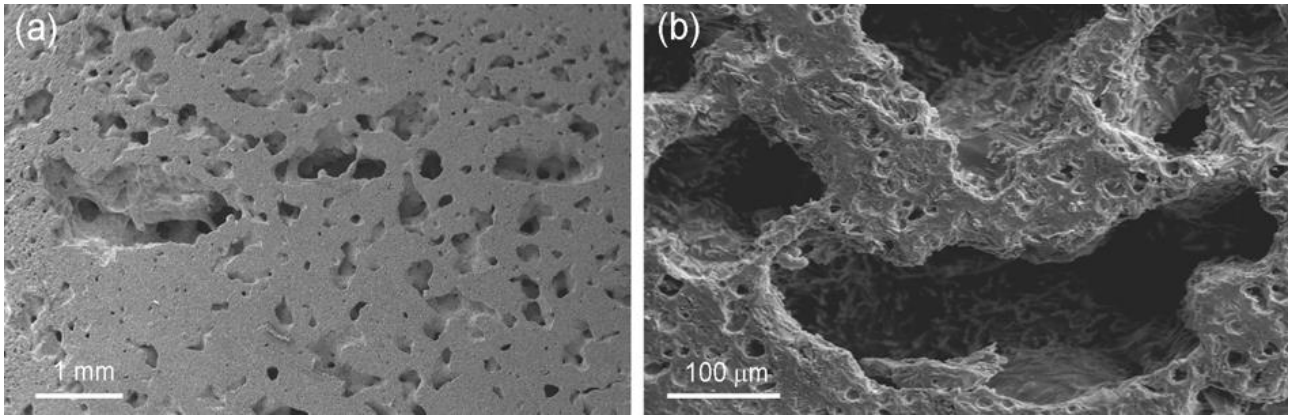

Fig. 7 Capillarity test carried out on FaGC-S-70

Fig. 8 Typical stress-strain curve of FaGC-S-70 (direction T1)

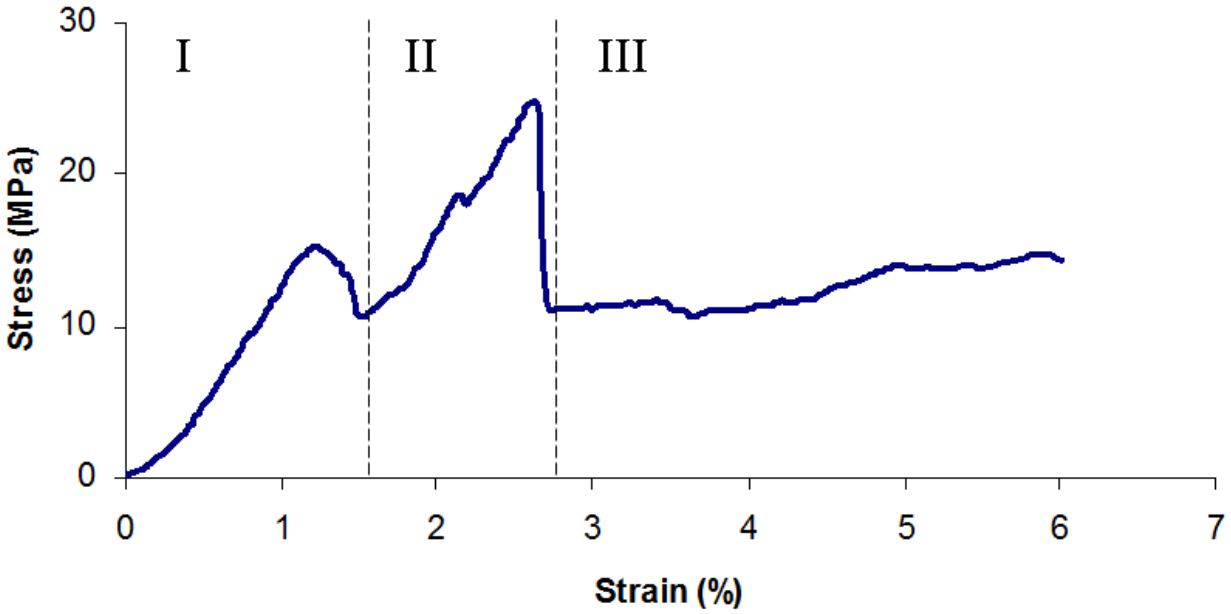

Fig. 9 PE grains deformation occurring during pressing: (a) FaGC/PE particles pressing and (b) resulting "green" compact

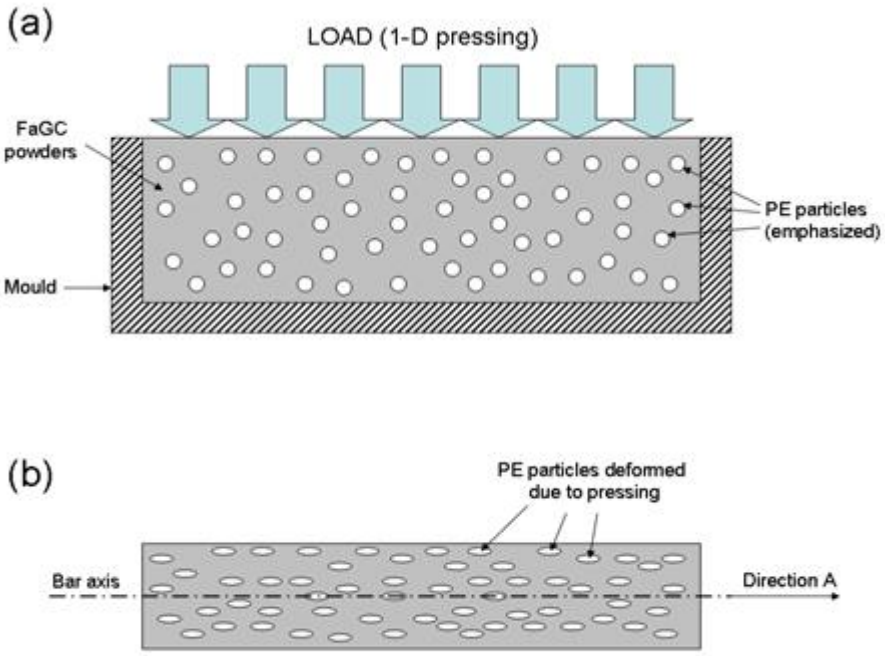

Fig. 10 *In vitro* bioactivity: (a) hydroxyapatite agglomerates on FaGC-S-70 walls after soaking for 7 days in SBF and (b) corresponding EDS pattern

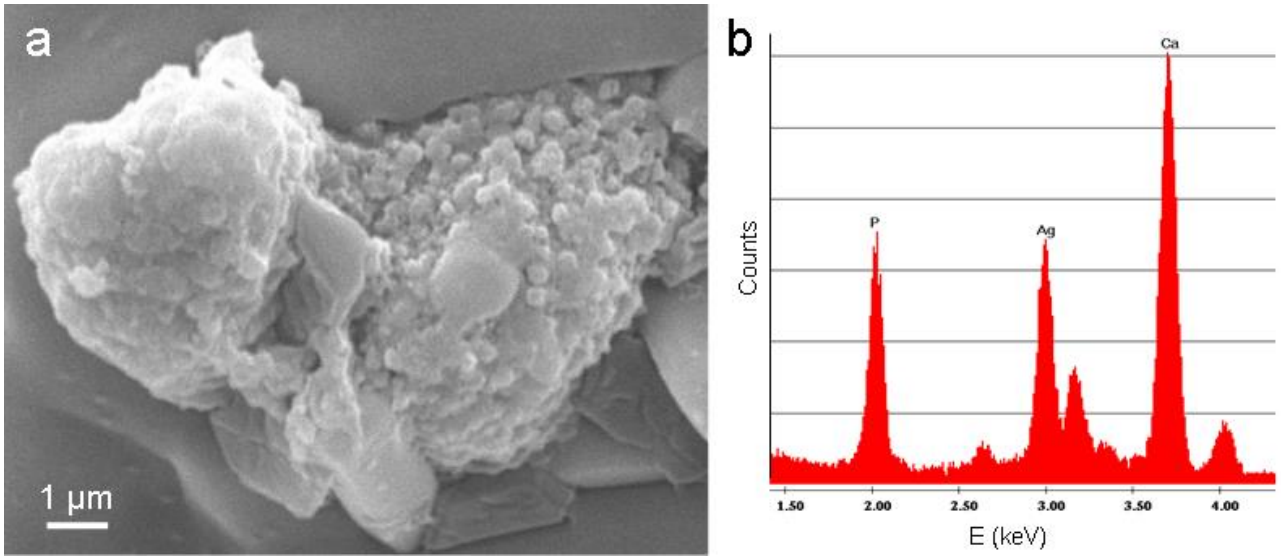

Fig. 11 Fitting curve for scaffold porosity: $\Pi^* = \Pi^*(P)$

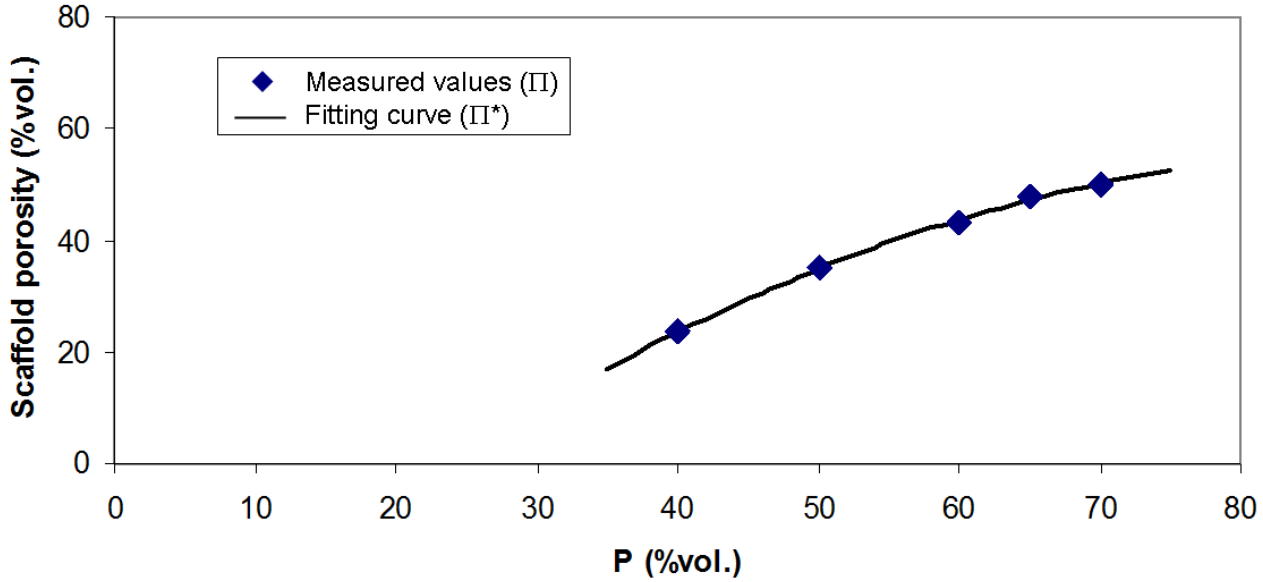

Fig. 12 Fitting curve for scaffold strength: $\sigma^* = \sigma^*(P)$

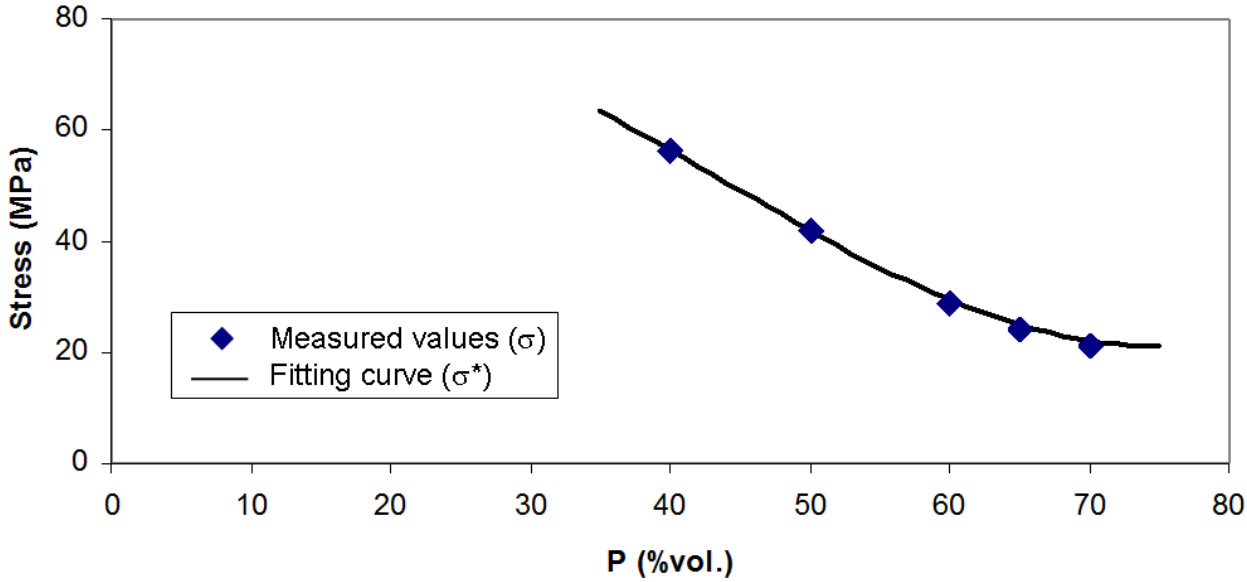

Tables

Table 1 Scaffolds porosity obtained via density measurements

Scaffold	Π (%vol.)
FaGC-S-40	23.5 ± 4.6
FaGC-S-50	35.0 ± 4.1
FaGC-S-60	43.2 ± 4.8
FaGC-S-65	47.8 ± 6.4
FaGC-S-70	50.0 ± 5.3

Table 2 Compressive strength of the scaffolds

Scaffold	σ_f (MPa)		
	Direction A	Direction T1	Direction T2
FaGC-S-40	148.1 ± 15.8	56.3 ± 3.2	54.8 ± 4.6
FaGC-S-50	130.6 ± 29.6	41.7 ± 4.8	39.2 ± 4.5
FaGC-S-60	118. 4 ± 22.1	28.8 ± 2.9	32.5 ± 4.8
FaGC-S-65	110.0 ± 23.8	24.3 ± 2.5	23.1 ± 3.0
FaGC-S-70	108.2 ± 32.7	21.0 ± 2.9	20.1 ± 2.2